Eur. Phys. J. B **51**, 277–284 (2006)
DOI: 10.1140/epjb/e2006-00221-y

THE EUROPEAN PHYSICAL JOURNAL B

Mo_6S_6 nanowires: structural, mechanical and electronic properties

I. Vilfan[1,a]

J. Stefan Institute, Jamova 39, 1000 Ljubljana, Slovenia

Received 6 April 2006
Published online 9 June 2006 –

Abstract. The properties of Mo_6S_6 nanowires were investigated with ab initio calculations based on the density-functional theory. The molecules build weakly coupled one-dimensional chains, like Mo_6Se_6 and $Mo_6S_{9-x}I_x$, and the crystals are strongly uniaxial in their mechanical and electronic properties. The calculated moduli of elasticity and resilience along the chain axis are $c_{11} = 320$ GPa and $E_R = 0.53$ GPa, respectively. The electronic band structure and optical conductivity indicate that the Mo_6S_6 crystals are good quasi-one-dimensional conductors. The frequency-dependent complex dielectric tensor ε, calculated in the random-phase approximation, shows a strong Drude peak in $\varepsilon_\parallel$, i.e., for the electric field polarised parallel to the chain axis, and several peaks related to interband transitions. The electron energy loss spectrum is weakly anisotropic and has a strong peak at the plasma frequency $\hbar\omega_p \approx 20$ eV. The stability analysis shows that Mo_6S_6 is metastable against the formation of the layered MoS_2.

PACS. 62.25.+g Mechanical properties of nanoscale materials – 73.22.-f Electronic structure of nanoscale materials: clusters, nanoparticles, nanotubes, and nanocrystals – 73.63.-b Electronic transport in nanoscale materials and structures

1 Introduction

Quasi one-dimensional materials like nanowires or nanotubes are attracting considerable interest, in particular because of their potential applicability in nanoelectronic and nanomechanical devices. Common to all of them is very strong uniaxiality in the electronic as well as mechanical properties, which is related to weak van der Waals coupling between individual molecular chains. They are very elastic, the strain at the (ultimate) tensile strength exceeds that of steel often by more than two orders of magnitude. As a consequence, they show extraordinary tensile strength along the long molecule axis — although the Young moduli are of the same order of magnitude. Perhaps even more challenging are their electronic properties. By tuning their bandgap or conductivity, one can build a series of very efficient and compact nanoscale electronic devices. In the past decade the research has largely concentrated on carbon-based nanotubes which often showed promising properties. Inorganic molybdenum-chalcogenide nanowires represent, as we shall see, a possible complementary or even alternative material with similar mechanical and electronic properties, but they are easier to prepare in clean, single-stoichiometry form.

As early as in 1980 Potel et al. reported on the synthesis of $M_2Mo_6S_6$ (M = K, Rb, Cs) [1]. These compounds all crystallize in the $P6_3/m$ space group with the Mo_6S_6 chains oriented parallel to the hexagonal c axis, located along the rhombohedral c edges and with the alkali metals in the $(2/3, 1/3, 1/4)$ and $(1/3, 2/3, 3/4)$ positions in the unit cell.

Molybdenum-chalcogenide crystals intercalated with Li ($Li_xMo_6Se_6$, $0 < x < 8$) or with other metals were also investigated in the past, e.g., as solid-state electrodes for secondary (rechargeable) lithium batteries, as one-dimensional conductors [2,3] and even as superconducting materials [4]. In the second example Li or Pb were needed to enhance the conductivity of nanowires. It seems that the extremely interesting mechanical properties of molybdenum-chalcogenide crystals were overlooked at that time. More recently, Ribeiro et al. [5] investigated the elastic properties and the band structure of $Li_2Mo_6Se_6$ by performing the ab initio total energy calculations. They pointed out the extraordinary high theoretical value of the Young modulus, comparable to the modulus of carbon nanotubes.

Other Mo-based nanowires, composed of Mo, chalcogens (S) and halogens (I) to form $Mo_6S_{9-x}I_x$ (Mo−S−I) have been investigated recently [6]. They have a skeleton of Mo_6 octahedra, each dressed with six anions (S or I), and bound together into chains by three anions (again S or I). Specific to these materials is growing in bundles of identical chains, large Young moduli, very small shear moduli, and easily controlled electronic properties.

[a] e-mail: igor.vilfan@ijs.si

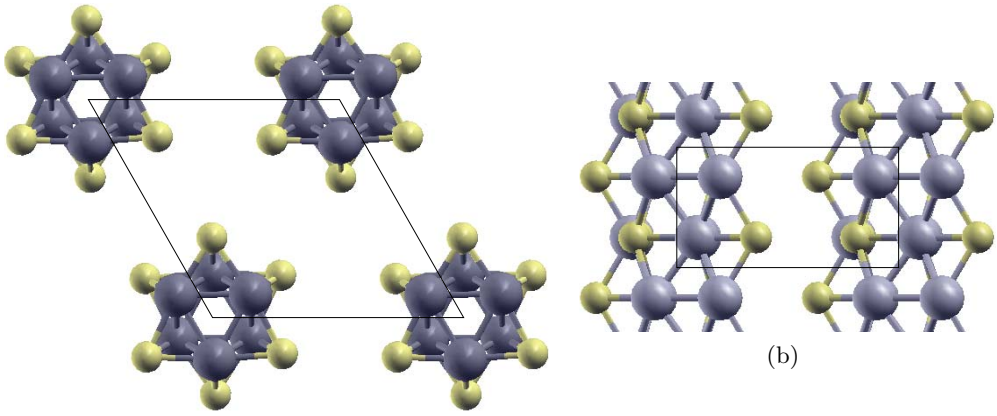

Fig. 1. The crystal of Mo_6S_6. (a) Top view (along the [0001] direction) and (b) side view (along the [1210] direction). Grey (dark) spheres: Mo, yellow (light) spheres: S. The Mo_6S_6 molecules form chains along the [0001] direction and a bundle of chains forms a nanowire. The separation between the chains is large and the interaction between them is weak, the Mo_6S_6 crystal is strongly anisotropic. In K_2Mo_6S6 the Mo_6S6 chains are rotated by $\sim 20^\circ$ in the anticlockwise direction and the K atoms are in the $(2/3, 1/3, 1/4)$ and $(1/3, 2/3, 3/4)$ positions.

In this paper we concentrate on the Mo_6S_6 (Mo−S) nanowires without and with intercalated K atoms. Using ab-initio total-energy and band-structure calculations we predict and discuss the stability, elastic and electronic properties of crystals made of Mo_6S_6.

2 Structure and computational details

The crystal structure of Mo−S is shown in Figure 1. The hexagonal crystals comprise one-dimensional chains oriented along the hexagonal c axis. Each chain is formed of a stack of Mo_3 triangles with staggered rotations and dressed with three anions (S). In order to clarify the stability, possible structures and properties of Mo−S nanowires we performed extensive density-functional theory (DFT) analysis using the WIEN2k code [7]. The simulations were performed on a mixed basis set of augmented plane waves plus local orbitals (APW+lo) for low orbital momenta ($\ell \leq 2$) and linearised augmented plane waves (LAPW) for all the higher orbital momenta [8]. The exchange and correlation potential was treated in the Perdew et al. generalised-gradient approximation (GGA) [9]. The muffin-tin radii were set to $R_{\rm Mo}^{\rm MT} = 1.06$ Å for Mo, $R_{\rm S}^{\rm MT} = 1.27$ Å for S and $R_{\rm K}^{\rm MT} = 1.32$ Å for K, the kinetic energy cutoff was $E_{\rm max}^{\rm wf} = 12.3$ Ry and the plane-wave expansion cutoff was $E_{\rm max}^{\rm pw} = 196$ Ry. The total energy was calculated on a mesh of 150 ($9 \times 9 \times 18$) k-points in the irreducible part of the Brillouin zone. The problem of the above DFT method is inappropriate treatment of the weak long-range van der Waals interaction which is responsible for bonds between individual chains in such molecular crystals. As a consequence, the DFT treatment of interaction between individual chains is not very reliable. On the other hand, the analysis of $K_2Mo_6S_6$ chains reveals that the calculated hexagonal lateral lattice constant a (at $T = 0$ K, as usual in the DFT calculations) differs from the experimental one (at room T) only by 2.6%, see Table 1. In any case, it is clear from both theory and experiment, that the lateral interaction between the chains is very weak. This is another reason why we shall concentrate on the intrachain structure and properties of single chains.

Table 1. The calculated lattice constants $(a, c)_{\rm calc}$ of Mo_6S_6 and $K_2Mo_6S_6$ and the experimental lattice constants $(a, c)_{\rm exp}$ of $K_2Mo_6S_6$ [1].

	Mo_6S_6	$K_2Mo_6S_6$
$a_{\rm calc}$	9.2 ± 0.1 Å	9.05 ± 0.1 Å
$a_{\rm exp}$	–	8.82 Å
$c_{\rm calc}$	4.35 ± 0.05 Å	4.43 ± 0.05 Å
$c_{\rm exp}$	–	4.44 Å

In the next stage, the total energy was minimised with respect to the internal atomic coordinates and to the hexagonal lattice constants a and c by assuming that Mo_6S_6 belongs to the same space group as $K_2Mo_6S_6$, i.e., $P6_3/m$ (176) [1]. This assumption is corroborated by weak coupling between individual molecular chains and by extensive analysis of Mo−S−I nanowires [6]. The space group $P6_3/m$ allows rotational relaxation of molecular chains around the c axis but does not allow mutual translations or deformations of chains along the c axis. The results of the energy minimizations of Mo_6S_6 and $K_2Mo_6S_6$ are compared with the available experimental lattice constants in Table 1. The structure of Mo_6S_6 is shown in Figure 1 and the interatomic distances in Table 2. In $K_2Mo_6S_6$ the calculated lattice constant $a_{\rm calc}$ is 2.6% larger than $a_{\rm exp}$, most probably because the DFT GGA overestimates the dispersive forces, acting between the chains. The nearest neighbouring distance between K atoms in $K_2Mo_6S_6$ ($d_{NN} = c$) is close to the interatomic distances in metallic K ($d = 4.53$ Å).

Table 2. Calculated ground-state interatomic distances in Mo_6S_6. The in-plane distances are between the atoms of the same Mo triangle with the adjacent three S atoms and the distances between the planes are between atoms in nearest neighbouring planes. The numbers in the last column are for $c = 4.63$ Å, ($\epsilon_{11} = 6.4\%$), i.e., close to the point where the chains start to break.

Bond		Distance	
		In equilibrium	Strained
Mo−S	In-plane	2.49 Å	2.46 Å
Mo−S	Between planes	2.62 Å	2.65 Å
Mo−Mo	In-plane	2.74 Å	2.67 Å
Mo−Mo	Between planes	2.69 Å	2.79 Å (2.782, 2.798)
S−S	Between planes	3.60 Å	3.66 Å
S−S	Closest interchain	4.22 Å	4.29 Å

The interatomic distances between the atoms of the same Mo_6S_6 chain are up to 8% longer than the intrachain distances reported for $Mo_6S_3I_6$ chains [6]. The in-plane Mo−Mo distance agrees, within the precision of our DFT calculation, with the experimental value for the room-temperature bulk metallic Mo (2.73 Å). In the Supplement of reference [6] an agreement within 0.1 Å between the room-temperature experimental distances in $Mo_6S_3I_6$ and the $T = 0$ distances calculated by the DFT was reported.

3 Results and discussion

To investigate the stability of the Mo_6S_6 and $K_2Mo_6S_6$ nanowires we performed also the DFT simulation of the layered MoS_2 compound and of atomic S and K in vacuum (i.e., one S or K atom in the unit cell $10.1 \times 10.6 \times 11.1$ Å^3 with periodic boundary conditions). The comparison shows that for Mo_6S_6 the energy difference with respect to the more stable MoS_2 is $\Delta E = E(Mo_6S_6) - 6E(MoS_2) + 6E(S) = 28$ eV (per one Mo_6S_6 unit) and tells us that the Mo−S nanowires with Mo in oxidation state 2 are, like other Mo−S−I nanowires, metastable against MoS_2 with the Mo oxidation state 4. The stability of Mo_6S_6 is comparable to the stability of already synthesised material $Mo_6S_3I_6$ for which the calculated energy difference is $\Delta E = E(Mo_6S_3I_6) - 6E(MoS_2) + 9E(S) - 6E(I) = 32$ eV. Per one atom, however, the energy difference is 2.33 eV for Mo_6S_6 and 2.13 eV for $Mo_6S_3I_6$. Therefore we expect Mo_6S_6 to be stable in air, in analogy with the Mo−S−I nanowires. The already synthesized $K_2Mo_6S_6$ is stable in air [1], the corresponding energy difference to MoS_2 is 21.0 eV and the Mo oxidation state is 2.33.

3.1 Elastic properties

The Mo-based nanowires and nanotubes have large elastic moduli in the direction of the wires and very small shear moduli in general [10]. To investigate the mechanical properties of the Mo−S nanowires, we performed DFT simulations for a series of lattice constants c. Due to weak interchain coupling the effect of a on the total energy is very small and was neglected unless otherwise stated. The lattice constant a was thus kept fixed during expansion, but the atomic positions were fully relaxed. For larger lattice constants, when the nanowires start to break, we simulated double cells, composed of two unit cells in the c direction, so that each simulated cell contained 12 Mo and 12 S atoms and the space group was reduced to $P\overline{1}$. In this way we reduced the effect of the interaction between breaking segments in a simulation with periodic boundary conditions. The results, presented in Figure 2 show the behaviour of the stress σ_{11} ($\sigma_{11} \propto \mathrm{d}E/\mathrm{d}c$ at constant a) under tensile strain ϵ_{11}. The initial slope yields for the elastic coefficient in the direction of the nanowire $c_{11} \approx 320$ GPa, which is larger than the Young modulus of steel but about three times smaller than for (single-wall) carbon nanotubes, see Table 3. Upon increasing strain, the slope decreases and eventually changes sign. Usually we say that the system breaks after σ_{11} reaches the maximum stress. Mo−S, however, behaves in a very different way. σ_{11} decreases after the first maximum, but then it starts to rise again until it reaches a local maximum. Breaking of Mo−S nanowires is thus a two-stage process, see Figure 3. In the first stage, the Mo−Mo bonds at some place are stretched until they break. In the second stage, the nearby S atoms move into the empty space between the chains and bind together the two ends of the wires until, eventually, also these Mo−S−Mo bonds and thus the whole chain breaks at the second maximum in Figure 2. Notice that the nonlinear regime below $\epsilon_{11} \sim 0.06$ in Figure 2 is the consequence of the anharmonic contributions to the interatomic potential and is not related to plastic deformation which is absent in our DFT simulations.

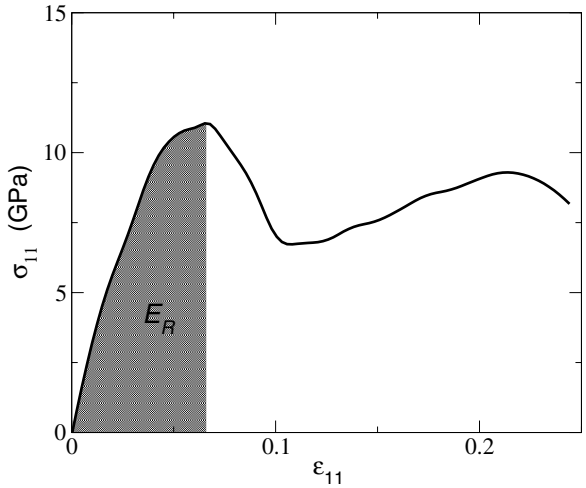

Fig. 2. Elastic properties of Mo_6S_6 nanowires. The elastic strain ϵ_{11} is for a unit cell, doubled along the c axis. At the first and second maxima the Mo−Mo bonds and the Mo−S−Mo bonds break, respectively. The initial slope of the curve defines the elastic modulus $c_{11} = 320$ GPA, and the grey area the modulus of resilience $E_R = 0.53$ GJ/m^3.

Table 3. Elastic properties of nanowires, carbon nanotubes (single-wall, SWCNT and multi-wall, MWCNT) and steel for comparison. Y is the Young modulus, E_R modulus of resilience, and T the tensile strength. The data for uniaxial systems are along the wires or tubes. The ideal tensile strength of Mo_6Se_6 is overestimated because it was assumed that the crystal stretches uniformly.

	Y (GPa)	E_R (GPa)	T (GPa)
Mo_6S_6	320	0.53	11
$K_2Mo_6S_6$ [a]	∼230		
Mo_6Se_6	250	3.1	26
SWCNT	1000	5 to 10	∼30
MWCNT	<1800		
Steel	210	$\sim 3 \times 10^{-3}$	0.4

[a] Calculated in this paper; [b] calculated using the data for an isolated molecular chain [5]; [c] compilation of data from references [11] and [12].

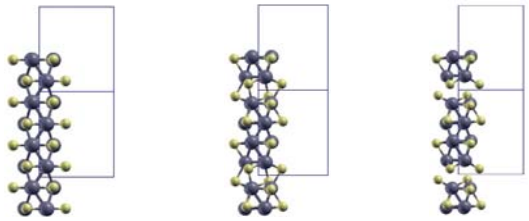

Fig. 3. Stretching of Mo_6S_6 nanowires is a two-stage process, as shown on this graph with two unit cells in the direction of the chain. (a) Fully elastic regime before the Mo−Mo bonds at a particular chain segment start to tear apart ($c = 4.60$ Å). (b) The Mo−Mo bonds between two neighbouring unit cells start to break and the S atoms move into the empty space between them by keeping the two ends of the broken chain together via four Mo−S−Mo bonds ($c = 4.975$ Å). (c) Eventually also the Mo−S−Mo bonds break ($c = 5.29$ Å).

The modulus of resilience, i.e., the maximal energy that can be *reversibly* stored in an elastic medium, is in our case equal to

$$E_R = \int_0^{\epsilon_{11}^{\max}} \sigma_{11} \mathrm{d}\epsilon_{11}. \qquad (1)$$

The Mo−S nanowires have a very high modulus of resilience, $E_R \approx 0.53$ GPa (see Tab. 3). This value is more than two orders of magnitude higher than for steel and already indicates possible applications of these nanowires: nanosprings. The *ideal* tensile strength, i.e., the maximal stress is $T \approx 11$ GPa, it is extremely high for an inorganic nanowire, but is by a factor of 3 smaller than for carbon nanotubes. Stretching the wire along the c axis by 6.4% causes a 3.7% elongation of the nearest interplanar Mo−Mo bond length and only a 2.6% contraction of the in-plane Mo−Mo bond length, see Table 2. The wire breaks at $\epsilon_{11} = 6.6\%$.

These are of course theoretical values. The experimental values of the tensile strength will be smaller due to lattice imperfections. Due to the almost one-dimensional structure and consequently small shear modulus, broken chains will diminish the tensile strength of an entire bundle of chains.

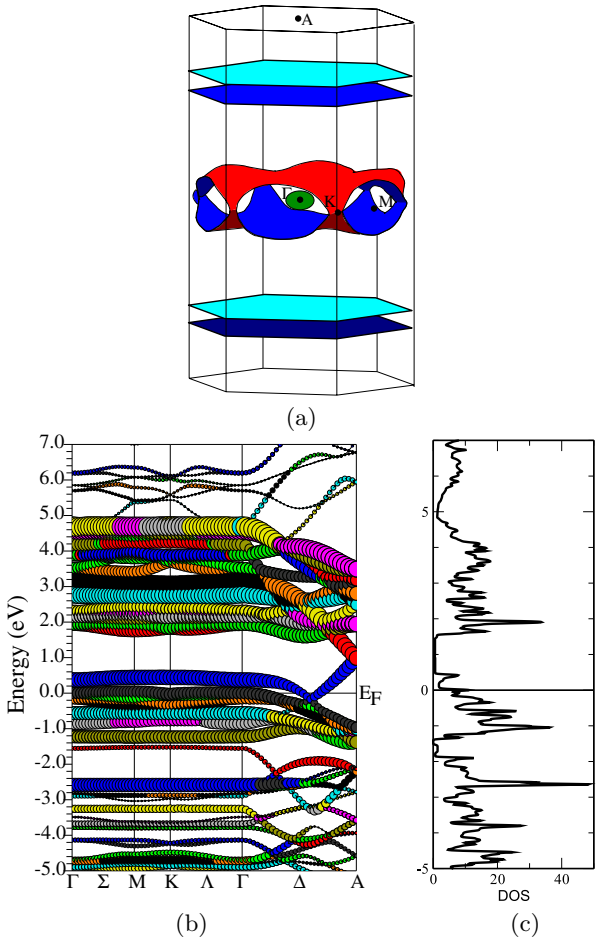

Fig. 4. (a) The Fermi surfaces in the Brillouin zone of Mo_6S_6 are very anisotropic and reflect the fact that the coupling between the molecular chains is weak. As a consequence, the electron group velocity points mainly parallel to the c axis. The letters show the positions of symmetry points in the Brillouin zone. (b) Electron band structure along the main symmetry directions. The dispersion of occupied states in the lateral direction is small, reflecting weak coupling between the chains. The radii of the circles indicate the Mo−4d character of the bands. The main contribution to the static charge-carrier transport comes from two bands, crossing the Fermi energy close to the Δ point. (c) The total electron density of states per eV in a unit cell.

3.2 Electronic properties

The basis of electronic and optical properties of Mo_6S_6 is the electron band structure, shown in Figure 4. For clarity, let us assign the sub-bands below −1.4 eV to the valence band and all the higher electron states to the conduction band. The Fermi energy then lies in the conduction band. Some of the sub-bands are doubly degenerated so that the conduction band carries 20 electrons per unit cell in total and all the valence bands together another

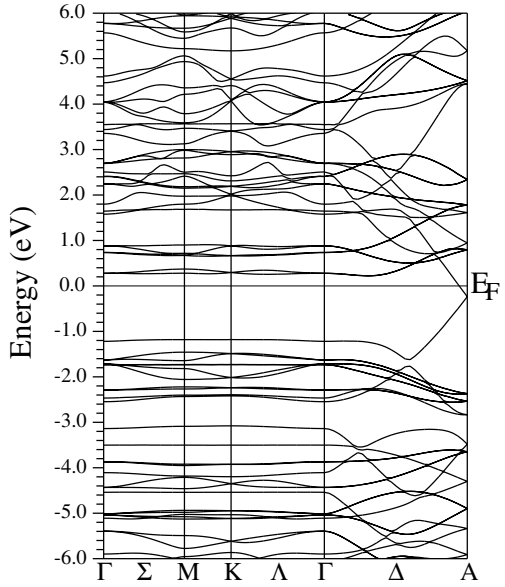

Fig. 5. Electron band structure of $K_2Mo_6S_6$ along the main symmetry directions. The main difference to the bandstructure of Mo_6S_6 is the shift in E_F.

52 electrons. These numbers agree with the total number of valence electrons in the unit cell: there are 12 atoms in the unit cell, each carrying 6 valence electrons. Due to the large number of equivalent atoms in the unit cell it is not possible to uniquely assign particular sub-bands to individual atoms. Some general observations can nevertheless be made. The band at −12.5 eV (not shown in Fig. 4) is clearly the 3*s*-band of S atoms. Between −5 and 0 eV we have a mixture of Mo-4*d* and S-3*p* bands, between 0 and 5 eV the bands have a clear Mo-4*d* character, whereas above 5 eV the S-3*d* states start to prevail. In the whole energy interval there is also a substantial contribution of interstitial electrons to the total density of states. For comparison, the band structure of $K_2Mo_6S_6$ is shown in Figure 5. The intercalation of K atoms does not alter the general shape and anisotropy of the bands which is still governed by the intrachain wavefunctions overlap. K atoms add two electrons per unit cell which occupy one band and shift the Fermi energy up by about 1.5 eV. The above band structures are also similar to the calculated band structures of Mo_6Se_6 and $Li_2Mo_6Se_6$ nanowires [5].

Dispersion of individual occupied sub-bands in the plane perpendicular to the wires is very small, of the order 0.2 eV and is similar in magnitude to the dispersion in Mo−Se and other Mo−S−I nanowires [5,6]. The reason for the small dispersion lies in weak, mainly Van der Waals coupling between the wires. Interestingly enough, even intercalation with K does not alter the dispersion in this plane noticeably. The conduction electrons are localised on individual wires and the hopping rates between the neighbouring wires are small. The dispersion in the direction parallel to the wires is more system-specific. In Mo_6S_6 there are four sub-bands crossing the Fermi energy E_F, thus building four Fermi surfaces, shown in Figure 4a. The first surface is a small, weakly anisotropic sphere close to the Γ point which makes very small contribution to the charge density at E_F and to the conductivity. The main contribution to the static charge carrier transport and to static dielectric properties comes from electrons at the upper two Fermi surfaces which cross the $\Gamma - A$ line close to the Δ point and are very flat as a consequence of anisotropic coupling between the wires. Thus, electrons in two sub-bands contribute to the static charge transport, the other either occupy sub-bands that don't cross the Fermi energy or have high effective mass. These two sub-bands have the dispersion in the direction parallel to the wires typical for nearly-free electrons. We find one electron sub-band starting at $E(\Gamma) = -0.73$ eV with an effective mass $m_{\|}^{\mathrm{el}} \sim 1.2m$ (m is the free-electron mass) and one hole sub-band starting at $E(\Gamma) = 0.37$ eV with an effective mass $m_{\|}^{\mathrm{h}} \sim 0.8m$. The slopes at E_F of these two sub-bands give the electron group velocity $v_{\|}^{\mathrm{el}} \sim 0.4 \times 10^6$ m/s and the hole group velocity $v_{\|}^{\mathrm{h}} \sim 0.6 \times 10^6$ m/s. The spin-orbit coupling — if added — neither splits the two sub-bands that cross the Fermi energy close to Δ nor does it alter noticeably the effective masses or the velocities of the two sub-bands. The values of $m_{\|}$ and $v_{\|}$ are of the orders of magnitude typical for metals, the Mo−S nanowires are thus candidates for one-dimensional ballistic quantum wires where the resistance is determined by the contacts of the wire. The ballistic regime is limited by the ability to produce defect-free nanowires, i.e., the length of the wire must not exceed the scattering length of the electrons. For a lifetime broadening of 0.01 eV (lifetime $\tau \sim 7 \times 10^{-14}$ s) this condition limits the length of the wires to ∼40 nm. As one-dimensional conductors, the Mo−S nanowires are also candidates for a Peierls transition to an insulator at low temperatures. However, we cannot give an estimate here because we did not investigate the electron-phonon interactions.

Let us compare the electron bands in Mo_6S_6 with those in Mo_6S_9 (three additional S atoms are ordered in triangles in the bridging planes between successive Mo_6 octahedra, see Ref. [6]) and in $Mo_6S_6I_3$ (in this case the Mo octahedra are "intercalated" with 3 I atoms instead of 3 S). In the latter two cases the sub-band dispersion in the z direction is smaller and the band structures have narrow gaps close but above the Fermi energy. The Mo-4*d* electrons in Mo_6S_6 build conduction channels along the chains which are interrupted in case of Mo_6S_9 and $Mo_6S_6I_3$. As a consequence, the Mo_6S_6 is expected to be a much better conductor than Mo−S−I chains of the type Mo_6X_9 (X is a combination of S and I).

3.3 Optical properties

During synthesis of Mo−S−I nanowires several different stoichiometries are obtained which then have to be purified in order to obtain a single-stoichiometry compound. Therefore it is essential to distinguish between them. To facilitate the characterisation of different stoichiometries we predict here also the optical properties of Mo_6S_6.

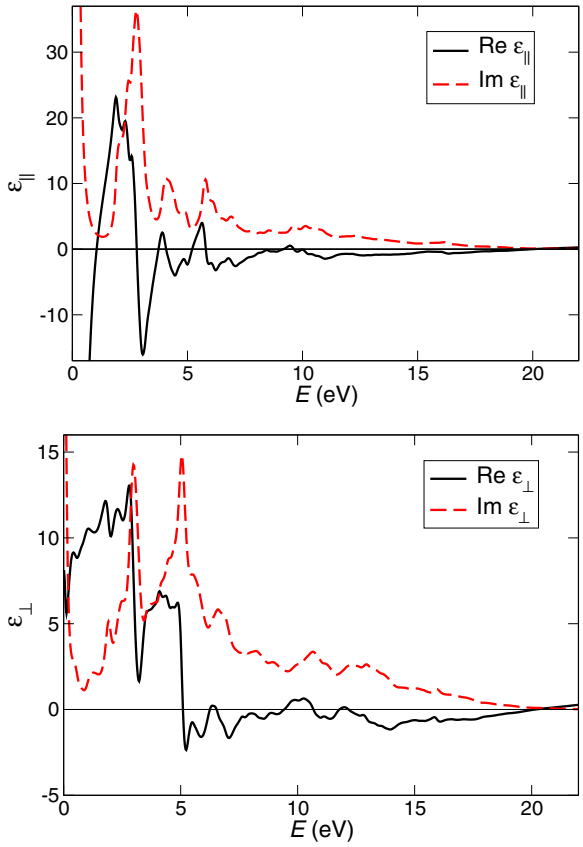

Fig. 6. Energy dependence of the complex dielectric functions $\varepsilon_\parallel$ and $\varepsilon_\perp$, broadened by a Lorentzian with $\Gamma = 0.1$ eV. The dielectric function $\varepsilon_\parallel$ has a pronounced Drude peak, typical for intraband transitions in metals, and an absorption peak at 2.8 eV. $\varepsilon_\perp$ shows two pronounced absorption peaks which are associated to the interband transitions and are closely related to the maxima in the joint density of states, which means that most of the sub-bands in the valence and conduction bands are a mixture of several symmetries, they have no unique band character. As a consequence, the selection rules are not very selective.

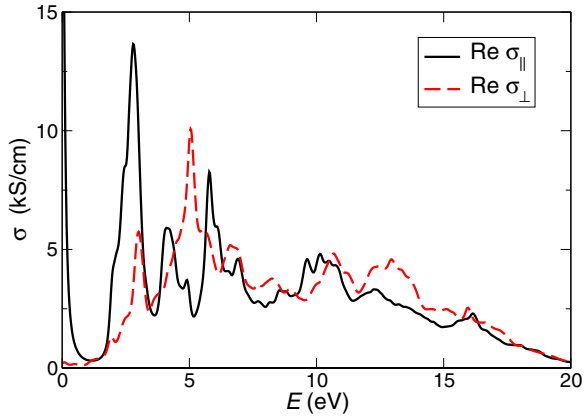

Fig. 7. Spectral dependence of the optical conductivity components $\mathrm{Re}(\sigma_\parallel)$ and $\mathrm{Re}(\sigma_\perp)$. Clearly seen is strong anisotropy in the static conductivity. The otherwise diverging peak at $E = 0$ was damped with $\Gamma_\parallel = \Gamma_\perp = 0.1$ eV to mimic the charge-carrier scattering.

We start with the frequency dependent complex dielectric function, Figure 6. The imaginary part of the dielectric tensor ε in the limit $q \to 0$ is calculated with the WIEN2k code on a tetrahedral mesh of 300 k-points in the irreducible part of the Brillouin zone and in the random-phase approximation [13]. The real part is then obtained from $\mathrm{Im}(\varepsilon)$ with the Kramers-Kronig relations. In our case the ε tensor is diagonal with the components $\varepsilon_{zz} = \varepsilon_\parallel$ and $\varepsilon_{xx} = \varepsilon_{yy} = \varepsilon_\perp$. The dielectric tensor has a Drude peak, associated with the transitions between the conduction electrons close to E_F, which is more pronounced in $\varepsilon_\parallel$. The anisotropy in $\varepsilon(E \to 0)$ is a direct consequence of the shape of Fermi surfaces. Above the Drude peak, $\varepsilon_\perp$ has two pronounced absorption peaks at 3 and 5 eV whereas $\varepsilon_\parallel$ has a structured absorption peak between 2 and 2.8 eV. These peaks are related predominantly to interband transitions between different S$-3p$ (below E_F) and Mo$-4d$ (above E_F) sub-bands. Above 5 eV the transitions are mainly to/from the S$-3d$ sub-bands. In all cases, however, the influence of interstitial electrons is large. Coming from the high-frequency side, $\mathrm{Re}(\varepsilon)$ changes sign (vanishes) at the plasma frequencies $\hbar\omega_{p\perp} = 20.1$ eV and $\hbar\omega_{p\parallel} = 20.0$ eV. The plasmons are *longitudinal collective excitations* of *all* valence and conduction electrons. ω_p agrees well with the estimate $\omega_p^2 = ne^2/\varepsilon_0 m$ (e is the electron charge, m its mass and ε_0 the permittivity of free space). With $n = 72$ valence electrons per unit cell of the volume $V = 317.6$ Å^3 we get $\hbar\omega_p = 17.6$ eV. The plasma frequency can be also tested with the f-sum rule,

$$\frac{\pi}{2}\omega_{p,i}^2 = \int_0^\infty \mathrm{Im}[\varepsilon_{ii}(\omega)]\omega \mathrm{d}\omega. \tag{2}$$

Numerical integration in the range from 0 to 41 eV gives $\hbar\omega_\perp = 18.5$ eV and $\hbar\omega_\parallel = 18.9$ eV. At the plasma frequency the effect of the anisotropy in the band structure on the dielectric tensor is small and ε is almost isotropic.

From ε we get the optical conductivity $\mathrm{Re}[\sigma(\omega)] = \varepsilon_0\omega\mathrm{Im}[\varepsilon(\omega)]$, see Figure 7. The static ($\omega \to 0$) peak is lifetime broadened due to the charge-carrier scattering mainly on impurities and imperfections in the crystal lattice. In the figure, the Drude peaks are broadened with $\Gamma_\parallel = \Gamma_\perp = 0.1$ eV, which corresponds to a lifetime $\tau \approx 0.7 \times 10^{-14}$ s. With such Γ the static conductivity along the wires is $\sigma_\parallel \sim 2 \times 10^4$ S/cm and the predicted anisotropy in σ is 100 : 1. At higher frequencies ($\hbar\omega > 5$ eV) the anisotropy in ε gradually disappears since the electrons are excited also above the ionisation threshold of 4.36 eV into the unbound (free) electron states.

The complex index of refraction $(n + \mathrm{i}k)$ with the components

$$n_{ii} = \sqrt{\frac{|\varepsilon_{ii}| + \mathrm{Re}(\varepsilon_{ii})}{2}} \tag{3}$$

and

$$k_{ii} = \sqrt{\frac{|\varepsilon_{ii}| - \mathrm{Re}(\varepsilon_{ii})}{2}} \tag{4}$$

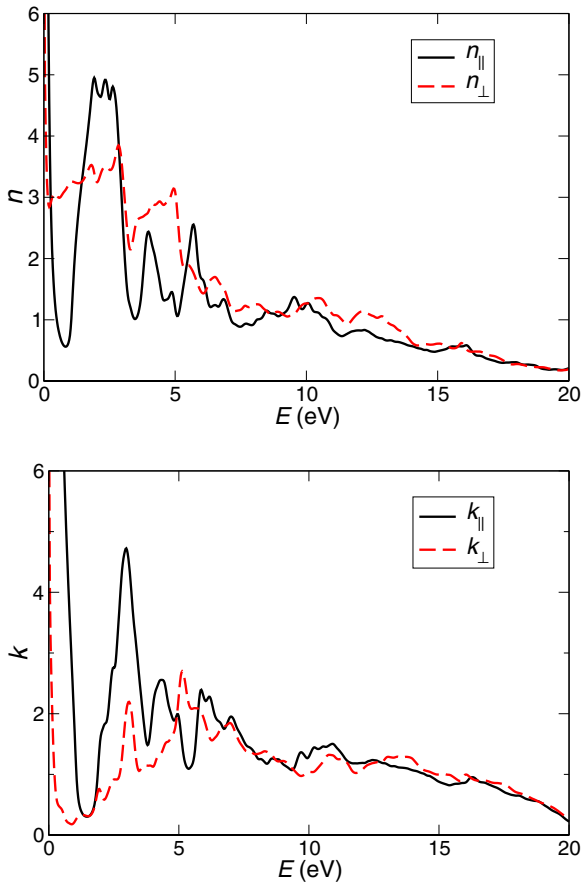

Fig. 8. Complex index of refraction $(n + ik)$, consisting of $n_\parallel$ and $n_\perp$ (upper panel) and extinction coefficients $k_\parallel$ and $k_\perp$ (lower panel).

is shown in Figure 8. It has similar trends as the dielectric function from which it is derived.

Finally, the electron energy loss function $L_{ii}(\omega) = -\mathrm{Im}\,(1/\varepsilon_{ii}(\omega))$ is shown in Figure 9. The pronounced peak at ∼20 eV lies very close to ω_p and is intimately related to the plasma excitations [14]; the effect of intraband transitions on this peak is small.

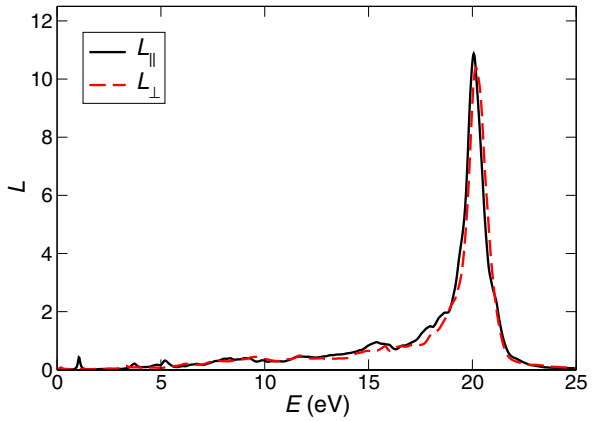

Fig. 9. Electron energy loss function L has a pronounced peak close to the plasma frequency $\omega_p \approx 20$ eV.

4 Conclusions

The aim of the paper is to stimulate synthesis and research on Mo_6S_6 and $M_2Mo_6S_6$ (M = alkali metal) which — according to our theoretical predictions — are good quasi-one-dimensional conductors and at the same time have high moduli of elasticity and resilience along the wires. This combination of electronic and mechanical properties makes them unique in the area of one-dimensional nanomaterials. The chains made of triangular Mo_3, surrounded with three S, build conduction channels along the hexagonal c axis with very weak "leakage" of the current between individual chains. The intercalated alkali metals contribute additional charge carriers and thus cause a shift in the Fermi energy but do not build their own conduction channels.

Synthesis of Mo_6S_6 should follow the guidelines to make the Mo_6Se_6 [2] whereas $M_2Mo_6S_6$ has been synthesized quite some time ago together with $M_2Mo_6Se_6$ [1]. Synthesis might be difficult since in particular the compounds with S are metastable against the much more stable layered MoS_2. Intercalation with alkali metals, if necessary to stabilise the compound, does not change the described properties qualitatively.

Mo_6S_6 and $M_2Mo_6S_6$ could be challenging alternatives to other nanomaterials like carbon nanotubes. The compounds have similar mechanical properties and thermal stability, they are stable to about 700 K in air (the thermal stability of Mo_6S_6 is believed to be comparable to the stability of other already existing Mo−S−I compounds). The advantage of Mo_6S_6 and $M_2Mo_6S_6$ could be that they are easier to synthesise in a clean, one-stoichiometry form and that they have better conductivity than carbon nanotubes, due to their purely molybdenum metallic chains. Mo_6S_6 is, according to the DFT results, also a better conductor and has better mechanical properties than the already synthesised Mo−S−I nanowires like $Mo_6S_{9-x}I_x$. One dimensional nature of the systems opens also the possibility of ballistic conduction or Peierls instability.

The author would like to thank D. Mihailovic for stimulating discussions. This work was supported by the Slovenian Research Agency under the contract P1-0044. The crystal structures were visualized by Xcrysden [15].

References

1. M. Potel, R. Chevrel, M. Sergent, J.C. Armici, M. Decroux, O. Fischer, J. Solid State Chem. **35**, 286 (1980)
2. J.M. Tarascon, J. Electrochem. Soc. **132**, 2089 (1985)
3. L. Venkataraman, C.M. Lieber, Phys. Rev. Lett. **83**, 5334 (1999)
4. R. Brusetti, P. Monceau, M. Potel, P. Gougeon, M. Sergent, Solid State Comm. **66**, 181 (1988)

5. F.J. Ribeiro, D.J. Roundy, M.L. Cohen, Phys. Rev. B **65**, 153401 (2002)
6. A. Meden, A. Kodre, J. Padeznik Gomilsek, I. Arcon, I. Vilfan, D. Vrbanic, A. Mrzel, D. Mihailovic, Nanotechnology **16**, 1578 (2005)
7. P. Blaha, K. Schwarz, G.K.H. Madsen, D. Kvasnicka, J. Luitz, *WIEN2k, An APW + LO Program for Calculating Crystal Properties* (K. Schwarz, TU Vienna, 2001)
8. E. Sjöstedt, L. Nordström, D.J. Singh, Solid State Comm. **114**, 15 (2000)
9. J.P. Perdew, K. Burke, M. Ernzerhof, Phys. Rev. Lett. **77**, 3865 (1996)
10. A. Kis et al., Advanced Materials **15**, 733 (2003)
11. M.-F. Yu, B.S. Files, S. Arepalli, R.S. Ruoff, Phys. Rev. Lett. **84**, 5552 (2000)
12. S. Ogata, Y. Shibutani, Phys. Rev. B **68**, 165409 (2003)
13. C. Ambrosch-Draxl, J.O. Sofo, e-print `arXiv:cond-mat/0402523` (2004)
14. D. Pines, Rev. Mod. Phys. **28**, 184 (1956)
15. A. Kokalj, J. Mol. Graphics Modelling **17**, 176 (1999), code available from `http://www.xcrysden.org/`